Progress and problems in reliability of Ti:$LiNbO_3$ optical intensity modulators

Hirotoshi Nagata
Junichiro Ichikawa
Sumitomo Osaka Cement Co., Ltd.
Optoelectronics Division
Central Research Laboratories
585 Toyotomi-cho
Funabashi-shi, Chiba 274, Japan

Abstract. The $LiNbO_3$ optical intensity modulator is a promising key device in global optical communication systems which demand high reliability. Although performance of the modulator has been considerably improved to meet practical use, there remain problems related to reliability issues such as unpredictable fluctuation of drift phenomena. In this regard, our recent experimental data on the fabrication of Ti:$LiNbO_3$ modulators are presented here to clarify problems in the device characteristics caused by the device materials. At present, there is little understanding of the origins and mechanisms of the fluctuations, and the estimation and assurance of device quality throughout the long term are difficult. In order to obtain as great a reliability as possible, screening tests for all produced devices are needed.

Subject terms: lithium niobate; modulator; reliability: drift.

Optical Engineering 34(11), 3284-3293 (November 1995).

1 Introduction

The $LiNbO_3$ optical modulator has become a promising key device for high-speed optical communication systems where a high device reliability is demanded. Such rapid progress in the development of $LiNbO_3$ devices was based on various engineering efforts to exclude intrinsic disadvantages in $LiNbO_3$ materials. For the mass production of these devices, 3-in.-diameter single-crystal wafers of congruent composition were commercially produced and used.[1–3] Recently, a further effort to eliminate proton impurities in the wafer was carried out by Koide et al.[4] Optical waveguides with low insertion loss were obtained via thermal diffusion of titanium ions into the wafer under a wet gas environment at a temperature close to the Curie temperature of $LiNbO_3$.[5–9] The photorefractive effect of $LiNbO_3$ could be significantly reduced for light wavelengths of 1.3 to 1.5 μm by decreasing the Fe^{2+} impurity and/or doping of Mg ions.[10] The pyroelectric effect, leading to thermal instability in the device, was prevented by the use of an *x*-direction oriented wafer and/or by shielding pyroelectrically induced charges with a semiconducting Si layer formed on the wafer surface.[11–14] Electrical relaxation phenomena caused by the dielectric nature of the materials, which is a possible origin of dc drift in the device, are known to be significantly reduced by the adoption of a proper buffer layer over the waveguides and by a decrease of proton impurities in the $LiNbO_3$ wafer.[15–21]

Many methods for coupling optical fibers to the $LiNbO_3$ waveguides have been proposed in order to obtain long-term endurance, even under temperature fluctuations from 0 to 70℃.[22] Furthermore, the $LiNbO_3$ device and fibers were hermetically packed in a metal package with dry gas, maintaining an He leak rate of less than 5×10^{-8} atm·cm^3/s.

In spite of progress toward the realization of $LiNbO_3$ devices, many problems remain concerning reliability issues. The origins and mechanisms of the drift phenomena which lead to inevitable fluctuation in the performance of the modulators have not been clarified yet. The quality of $LiNbO_3$ crystal wafers needs to be standardized for production use, and Minakata has undertaken a useful investigation and has made some proposals.[23] Test procedures and criteria for quality assurance of the $LiNbO_3$ modulators have not been determined while those for semiconductor-based optical devices are commonly adopted. These problems must be discussed and solved before the use of $LiNbO_3$ devices in optical communication systems becomes practical. This article reports on recent progress and remaining problems on the $LiNbO_3$ optical intensity modulators, which were obtained from our experiments and experience in the fabrication of devices.

2 Device Structure and Fabrication

2.1 *$LiNbO_3$ Wafer*

Commercial 3-in.-diameter and 0.5-mm thick z-cut $LiNbO_3$ wafers were used to fabricate Mach–Zehnder-type interferometric optical intensity modulators. The wafers were cut from a crystal boule synthesized by a conventional technique; they contained the inevitable proton contaminations, which were mainly introduced during the poling process of the crystal.[24] The protons were reported to exist at particular sites in O-O planes of $LiNbO_3$ crystal and were measured by a Fourier transform infrared transmission (FTIR) spectrometer with -OH absorption peaks at 3400 to 3500 cm^{-1}.[25–30] Table 1 shows the OH contents in the z-cut wafers sliced from the same crystal

Paper 23015 received Jan. 20, 1995; revised manuscript received Apr. 27, 1995; accepted for publication Apr. 27, 1995.

Table 1 Proton (OH ion) contents in commercial $LiNbO_3$ wafers cut from the same crystal boule measured by FTIR. Sample numbers correspond to the *z* direction of the crystal boule (the sign of the direction was not known). The measurements were done at five points in the wafer; i.e., at the center, $\pm y$, $-y$, $+x$, and $-x$ sides of the 3-in. wafer. The values are the absorption coefficients (cm^{-1}) for OH mode while the values in the parentheses are molar contents of OH ions calculated from the formula reported by Bollmann (Ref. 25).

Sample no.	Center	+y	-y	+x	-x
ZG807271-5	1.5486	1.6956	1.7331	1.6889	1.6039
	(7.7×10^{-5})	(8.5×10^{-5})	(8.7×10^{-5})	(8.4×10^{-5})	(8.0×10^{-5})
ZG807271-16	1.7831	1.8425	1.8184	1.8190	1.8231
	(8.9×10^{-5})	(9.2×10^{-5})	(9.1×10^{-5})	(9.1×10^{-5})	(9.1×10^{-5})
ZG807271-29	1.8192	1.8857	1.7996	1.8246	1.8231
	(9.1×10^{-5})	(9.4×10^{-5})	(9.0×10^{-5})	(9.1×10^{-5})	(9.1×10^{-5})

boule. The OH mole fractions in Table 1 were calculated from the measured absorption constants using the equation reported by Bollmann.[25] The observed OH peaks were at 3489 cm^{-1} (main peak) and 3471 cm^{-1} (subpeak), which were close to those reported for Li-deficient crystals.[29] The results exhibited a simple change of the proton contents along the *z* axis of the crystal. This phenomenon was possibly caused by an electromigration of the ions during the poling process at high temperature, as reported by Smith.[24] Further, if the protons diffused throughout the crystal, its contents should show a distribution in the wafer that depends on crystal defects. Table 1 also exhibits such results measured at several points on the 3-in. z-cut wafer. A small distribution of the proton contents was found in the wafer.

The proton contents of the $LiNbO_3$ substrate influenced the electrical nature of the material, such as resistance and drift phenomena of the device. As described later, the modulator made from the reduced proton $LiNbO_3$ wafer exhibited smaller dc drift than that from the wafer used here.[19] Similar results were reported on a $LiNbO_3$ optical switching device.[21] In this regard, the above-mentioned distribution of the proton contents in the wafer, which occurred unexpectedly, might be one of the reasons for unpredictable fluctuation in the drift phenomena observed, even in modulators made from the same wafer lot.

Recently, a significant improvement of the waveguide surface morphology was reported using proton-free $LiNbO_3$ wafers, even after (dry) heat treatment.[31] The OH IR absorption coefficients measured on two such z-cut wafers were 0.06 to 0.08 and were about only 5% of those measured on the wafers used here.

2.2 *Waveguide Formation*

The Mach–Zehnder-type waveguides designed for 1.5-μm wavelength light propagation were formed on a – z face of the wafer along the *x* direction by a conventional thermal indiffusion of Ti. The length of the waveguide was about 60 mm, including the 40-mm long symmetric Mach–Zehnder arms. Prior to the diffusion process, a metallic Ti layer 76 to 80 nm thick was deposited by a vacuum evaporation technique, and was patterned by a conventional photolithography technique. These wafers were heat treated at 980℃ for ~20 hr in a flow of wet O_2/N_2 mixture (synthesized air) which was introduced into the furnace by a water bubbler at room temperature.

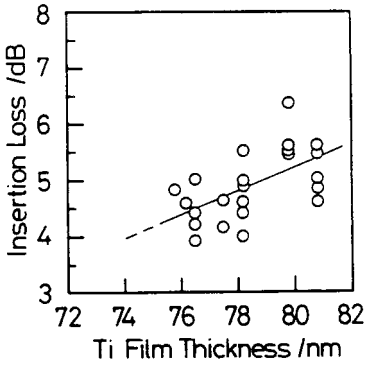

Fig. 1 Relation between optical insertion losses of the assembled modulators and thicknesses of metallic Ti layers for the waveguide formation. The measured insertion losses included the losses resulting from the waveguide design and coupling with optical fibers.

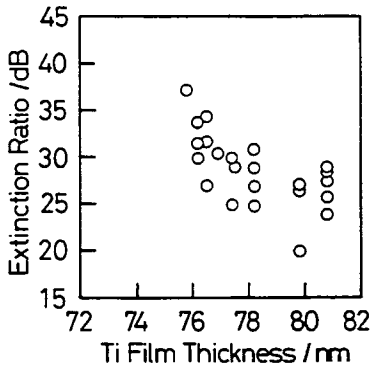

Fig. 2 Relation between extinction ratios of the modulator optical outputs and thicknesses of metallic Ti layers for the wavegide formation.

Figure 1 shows the relation between optical insertion losses of the modulators and deposited Ti layer thicknesses. The insertion loss was measured on the assembled modulator and consisted of losses due to the waveguide itself, mainly, and also to the coupling between the waveguide and the optical fiber via adhesive materials, etc. The thickness of the Ti layer was measured before the diffusion process by a stylus method. The data scattered within $\pm$ 0.5 dB, but exhibited a clear tendency toward a nearly proportional relationship of the loss against the Ti deposition thickness. A similar dependence concerning the thickness of the Ti layer was observed in the on/off extinction ratio of the modulators, as shown in Fig. 2. These results suggested that the thickness (i.e., amounts) of Ti to be indiffused was a sensitive factor affecting the waveguide characteristics, especially the optical insertion losses, in addition to the critical humid condition for heat treatment.

In the present experiments, the surface morphology of the waveguide with reduced optical loss, which was prepared from a thinner Ti layer, showed significantly improved surfaces. The increase of loss values corresponded to a deterioration of

the surface caused by a steplike growth of crystalline precipitates. As a reason for surface roughening during the heat treatment, outdiffusion of Li and epitaxial growth of the $LiNb_3O_8$ phase on $LiNbO_3$ have been reported.[32–35] However, from the present degraded waveguides, no additional x-ray diffraction peak was detected by a conventional $\theta/2\theta$ scan technique and the origin of the surface precipitates is not known yet. Consequently, fabrication parameters for waveguides with smooth morphology and low optical insertion loss seemed to be restricted within a narrow tolerance. Koide et al. recently investigated how the influence of the dew point of flowing gas on Ti thermal diffusion affects the surface morphology and obtained refractive indices as a function of the initial proton contents in the wafer, suggesting the possible fabrication of excellent waveguides, even by a dry annealing.[31] Furthermore, it was found that precise control of the Ti layer thickness, on the order of 2 nm for the present case, was necessary to repeatedly produce devices with a low optical insertion loss.

2.3 *Formation of SiO_2 Buffer and Electrode Layers*

An SiO_2 buffer layer was deposited over the Ti:$LiNbO_3$ waveguides by vacuum evaporation and annealed at 600℃ for 5 hr in flowing wet O_2. The layer thickness was set to be 1 μm for modulators with a bandwidth of 5 to 10 GHz. The density of the present SiO_2 layer was less than that of an alternative one deposited by an rf-sputtering method, judging from its smaller refractive index. However, from the viewpoint of long-term reliability,[18] the vacuum-evaporated buffer layer made possible modulators with significantly reduced dc drift, as previously reported by the authors and also described in this paper.

Because of the thickness of the SiO_2 layer, the wafer was warped as a convex waveguide face, mainly because of the compressive thermal internal stress of the SiO_2 layer. Such bending of the waveguide caused a fluctuation in the refractive index and the operating point of the modulator optical output, via the piezo-optical effect of $LiNbO_3$.[36] In order to decrease this phenomenon, an additional SiO_2 layer was formed on the opposite side of the wafer in an attempt to cancel the wafer warping. For instance, a wafer with a 1.3-μm-thick SiO_2 layer was warped to show 32 μm of a deflection at the center of the wafer. However, the deflection was reduced to 8 μm by a deposition of 1.3-μm-thick SiO_2 on the back face of the wafer.

Figure 3 shows the distribution of the operating point at 30℃ on the modulators made from the same wafer with the buffer layers 1.0 μm thick for the front face and 1.24 μm thick for the back face. The operating point voltage was measured at 1 kHz operating with 1.5-μm wavelength light and was determined to be that for the optical output peak closest to the zero-bias point. The horizontal axis of the figure denotes the chip number of the modulators, whose width was about 1 mm (along the *y*-direction of the wafer). Because the operating point voltages were sensitive to the history of the device, such as bias and heat applications, via dc and thermal drift phenomena, the measured data of Fig. 3 included such extrinsic fluctuations. However, the extent of the distribution was considerably large and comparable with a half wavelength driving voltage (V_π) of the modulators. It is noted again that one of the origins of the fluctuation of the operationg points was internal stress in the waveguide that was caused by deposition

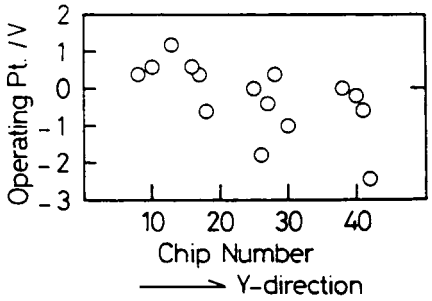

Fig. 3 Distribution of the operating points of modulator optical outputs for the samples made from the same wafer. The horizontal axis denoted as the device chip number corresponds to the *y* direction of the wafer.

of the coating layers.

The Au electrodes were formed by vacuum deposition and electroplating techniques on the Si thin layer which was formed on the SiO_2 buffer layer. This Si layer worked as a shielding layer for the pyroelectrically induced charges, reducing the thermal drift of the device, as reported by Seino et al.[11] The Au electrodes were 10 to 15 μm thick in order to achieve a velocity matching of microwaves and a high bandwidth. It was difficult to mechanically stabilize such thick electrodes with minimized internal stresses, especially for a hot electrode, which is asymmetric, with only ~10 μm width compared with 40 mm of length. Therefore, there have been some failures such as the peeling off of the hot electrode while the wafer was being cut into chips. For instance, due to weakening of the adhesion by partial oxidization of the Ti layer during the process, the electrode separated from the device at the interface between Au and Ti, which was deposited directly on the Si layer to improve the bonding strength of the Au and the Si. When the electrode was intentionally removed, the fracture occurred at the $SiO_2/LiNbO_3$ interface. This was perhaps caused by weak bonding of the interface as a result of surface contamination and a difference in the chemical bonding configuration of each layer (covalent and ionic bonds).

2.4 *Device Assembly*

The $LiNbO_3$ wafer, consisting of the Mach–Zehnder waveguides, SiO_2 buffer layer, Si layer, and Au asymmetric coplanar electrodes, was cut into chips about 0.8, 0.5, and 60 mm in width, thickness, and length, respectively. The end faces of the waveguide were finely polished during the same cutting process, in which conditions such as cutting speed were accurately adjusted.[22, 37] At one end of the waveguide (chip), a laminated polarizer was attached with a UV-curable low refractive index adhesive material in order to achieve higher extinction ratios. The chip was bonded in a Au/Ni plated stainless steel (AISI 303) package with a commercial epoxy adhesive containing Ag electroconducting fillers. This mounting structure eliminated the thermal fluctuation of the device, which was possibly caused by differences in the thermal expansion of the materials.[38] The electrodes were connected to a commercial rf feedthrough which had been hermetically soldered to the package.

Optical fibers were aligned to the waveguides and bonded together with the UV-curable adhesive materials, and the bond-

ing strength was reinforced using an additional $LiNbO_3$ block and a glass bead. The exposed surface of the fiber had been metallized with Au/Ni by a conventional electroless plating technique, and was Pb/Sn soldered to the feedthrough tube of the package for hermetic sealing. This component and its lid were seam welded and packed with a dry N_2/He mixture having a dew point of < -40℃. The He was introduced partially as a tracer gas for a fine-leak test of the package hermeticity. The He equivalent leak rate of such hermetically sealed packages must be less than 5×10^{-8} atm · cm^3/s. If a large leak existed in the package of the present device, a short circuit of the electrodes would occur during the operation under humid conditions. In the experiment using unsealed modulators, in which they were operated with dc 5-V bias voltage at 80℃ and 95% RH for a few hours, electrochemical reactions proceeding between the Si layer and Au electrodes, resulting in the short circuit due to the growth of Au/Si-based materials between the hot and ground electrodes. The hermetically sealed devices could endure electrostatic discharge (ESD) tests at levels of 500, 1000, 2000, and 4000 V.

2.5 *Screening Tests of the Modulators*

Screening tests were necessary for the present $LiNbO_3$ modulators to exclude devices with unpredictable fluctuations in their characteristics. The tests focused on thermal drift within an ordinary operating temperature (0 to 70℃), dc drift at high temperature (80℃), changes of optical insertion and return losses after the high-temperature aging, and package hermeticity. The problems associated with the optical losses and hermeticity were ascribed to the fiber assembly process and will be reported elsewhere.[39] In the following sections, problems in the drift phenomena are discussed as reliability issues of the current $LiNbO_3$ devices.

3 Thermal Drift Phenomena

3.1 *Backgrounds*

The operating point of the light-modulation output of the devices drifted due to a change of environmental temperature. Such thermal drift phenomena of the $LiNbO_3$ modulators were mainly induced by pyroelectric charges of the substrate caused by temperature changes. These undesirable charges could be shielded out and homogeneously distributed over the device surface by the effect of the Si layer, significantly decreasing the magnitude of the drift. Further, Nayyer and Nagata found residual thermal drift due to the total electric fields applied asymmetrically to the Mach–Zehnder waveguide arms, and improved it by the adoption of asymmetric waveguide arms.[40] Their report noted that the optical output followed a sinusoidal square variation with temperature, and that the proper introduction of asymmetric waveguide arms was helpful in adjusting the slope at its operating points, resulting in the suppression of the thermal drift. The modulators used here consisted of the symmetric Mach–Zehnder arms, however, and exhibited 2 to 3 V of the thermal drift while their V_π was ~ 3.5 V between 0 and 70℃.

Thermal drift, the very slow drift phenomenon that succeeded spontaneous drift, was sometimes found at high temperatures. This slow drift occurred in a direction opposite to the spontaneous one and was accelerated by a temperature rise. Figure 4 shows an example of such drift phenomena which was observed during the ac 1-kHz operation under a

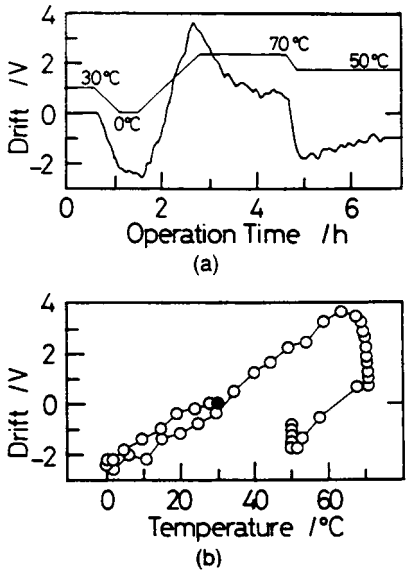

Fig. 4 (a) Example of the thermal drift of the modulator measured with heating and cooling rates of 1 K/min. (b) Replot of the data in (a) as the drift voltage versus the temperature.

Table 2 Results of thermal drift measurements for modulators with various hot/ground (H/G) electrode resistances. The rates (temperature coefficients) of the spontaneous drift during the heating process and the magnitudes of subsequent slow drift during the aging process are listed. The H/G resistances were measured at room temperature (~28℃).

Existence of Si layer	H/G resistance [Ω]	Spontaneous drift rate [mV/K]	Slow drift magnitude [V]
yes	71 k	42	< 0.5
yes	120 k	74	~ 0.5
yes	1.7 M	63	~ 2.5
yes	3.8 M	43	~ 0.5
yes	7.9 M	79	~ 3.0
yes	59 M	50	< 0.5
yes	3.7 G	64	~ 6.0
no	>> 10 G	110	~ 4.0
no	>> 10 G	300	~ 9.0

temperature change profile, as in Fig. 4(a) with heating and cooling rates of 1 K/min. The data were replotted as a relationship between the drift voltage of the operating point and the temperature in Fig. 4(b). Table 2 shows the rate (i.e., temperature coefficient) [mV/K] of the spontaneous drift between 30 and 70℃ and the magnitude [V] of the slow drift during 2 hr of soaking at 70 ℃, which was measured for various modulator samples with different electrical resistances between the hot and ground electrodes. The last two samples in the table did not have the Si layers. Between 30 and 70℃, the spontaneous drift seemed to be in proportion to temperature rises. Consequently, these drift rates were almost independent of

the resistance of the Si layer. Even for the modulators without Si layers, the drift rates were observed to be much slower than the results reported by Skeath for a similar device.[14]

One of the reasons for these results was that the exposed $LiNbO_3$ surfaces of the present modulators were very narrow, 25 μm along both sides of the 40-mm-long hot electrode, and, the magnitude of the localized pyroelectric charges could be reduced absolutely. On the other hand, the slow drift at 70℃ could not be reduced by formation of the Si layer. The origins of the slow drift have not been clarified yet, although it was found empirically that a difference in the way the SiO_2 buffer layer was formed affected the results. The buffer layers of some samples in Table 2 with larger drift had been heat treated once after the 1-μm-thick deposition, while others had been heat treated twice after each 0.5-μm deposition. One possible cause was the relaxation of the pyroelectrically induced charges caused by the dielectric nature of the materials, as well as the origins of the dc drift.

Finally it is noted that the rate of the spontaneous thermal drift depended slightly on the fluctuation in the operating point of the optical output, as previously reported.[38] This was caused by the almost constant thermal dependence of the V_π, which could be predicted from a thermal coefficient of the r_{33} electro-optic constant for z-cut $LiNbO_3$. For instance, a change of the V_π from 0 to 70℃ was measured as – 0.0016 V/K and close to – 0.0021 V/K from the calculation. For practical convenience, the drifts were measured at the optical output peak nearest to the zero bias point (i.e., within $\pm V_\pi$).

3.2 *Distribution of Thermal Drifts in Wafers*

Figure 5 shows the distribution of the spontaneous drift rates between 30 and 65℃ obtained for three different wafers, which are denoted by open circles, triangles, and closed circles in Fig. 5(a) and 5(b). These data were measured under a fast heating rate of 1 K/min to prevent the influence of the slow drift at higher temperatures. The extent of the distribution in the same wafer [see Fig. 5(a)] was large and comparable with

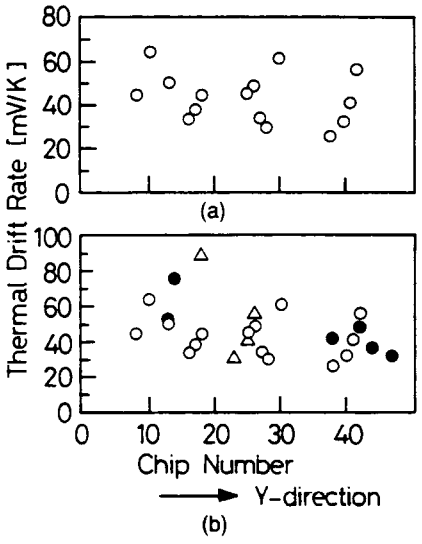

Fig. 5 Distributions of the spontaneous thermal drift rates between 30 and 65℃ of the modulators made from the same wafer (a) and made from three different wafers (b). The measurements were done with a heating rate of 1 K/min.

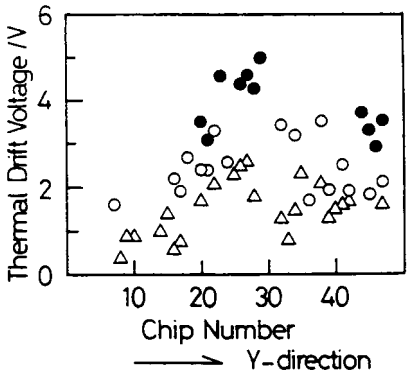

Fig. 6 Typical thermal drift, including both spontaneous and slow drift, measured by a routine method with a steplike heating profile.

those in the other wafers [see Fig. 5(b) and Table 2]. The maximum-to-minimum ratio of these fluctuations was in the range of 3 to 1, corresponding to a difference of 3 V within the ordinary temperature (0 to 70℃) range.

The other examples of such distribution are shown in Fig. 6, where the thermal drift was measured under a steplike heating profile between 0 and 70℃ with a 5-min soaking period for every 10 K increase. The results included both the spontaneous and slow drifts, and did not exhibit a linear relation against the temperature. The maximum drift voltages within this temperature range extended up to 5 V, where a criterion of the screening test was generally set at a voltage less than V_π (~3.5 V). Such inferior devices must be rejected before shipping.

3.3 *Possibility of Reduced Thermal Drift Modulators*

The magnitude of the spontaneous thermal drift seemed to depend significantly on the configurations of the electrodes and waveguides. Even in the *x* direction-oriented modulators with a symmetric electrode configuration, which exhibited negligible pyroelectric effect and significantly smaller thermal drift than the z-cut ones, the Si layer coating was effective in further reducing the drift phenomena. On the other hand, a dual hot electrode modulator[41] using the z-cut wafer produced little thermal drift. The typical results for these modulators measured by us, between 0 and 70℃ with heating and cooling rates of ± 1 K/min, are shown in Fig. 7(a) for the dual hot electrode sample and Fig. 7(b) for the x-cut one.

To reduce the drift of the modulators with asymmetric hot and ground electrodes, introduction of asymmetry into the Mach–Zehnder waveguide arms was proposed by Nayyer and Nagata.[40] The low extinction ratios, which were a disadvantage of the asymmetric arms, were significantly improved compared with the present symmetric arms.[42] However, an unexpected large hysteresis of the drift between heating (positive drift voltage of ~5 V between 20 and 70℃) and cooling (negative drift voltage of ~ – 1 V) was observed in these modulators, as typically shown in Fig. 8, which must be solved before practical application. The vertical axis (bias voltage) of Fig. 8 denotes the voltage for a specific light-modulation output peak at various temperatures. A change of these bias voltage values caused by temperature changes corresponds to the thermal drift voltage. The modulator of Fig. 8 was composed of a 7-μm-wide waveguide arm (as a width of the Ti pattern before its diffusion) under the hot electrode and a 6-

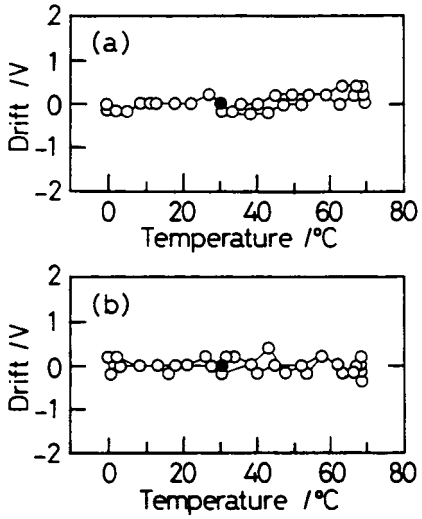

Fig. 7 Examples of the measured thermal drifts of dual hot electrode z-cut modulator (a) and of an x-cut modulator (b). Both modulators included the Si thin layers under the electrodes.

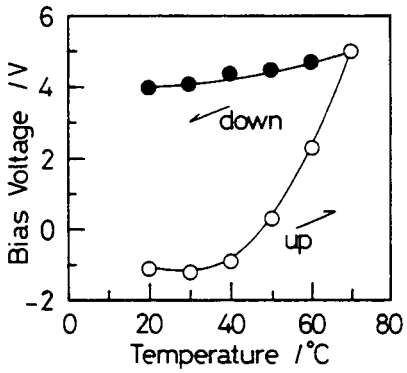

Fig. 8 Example of thermal drifts of a z-cut modulator with asymmetric Mach–Zehnder arms and symmetric electrodes. The measurements were carried out both for heating and cooling temperture steos.

μm-wide arm under the ground electrode. The thicknesses of the SiO_2 buffer and Si layers were 1.5 μm and ~100nm, respectively. The V_π, extinction ratio, and optical bandwidth of this modulator were measured at 4.32 V, 21.1 dB, and 11.4 GHz, respectively.

4 dc Drift Phenomena

4.1 *Experimental background*

The dc drift of the operating point of the light-modulation output was superimposed on the thermal drift, as shown in Fig. 9, in which the drift voltage of the specific operating point was measured and plotted with a temperature change profile. Figure 9(a) shows the result measured without any dc bias application, while (b) shows the result measured with a 5-V dc bias application. Figure 9(c) represents the subtraction of the data of (a) from (b), indicating the drift that is due to the dc bias application and not to the temperature change. This drift was saturated while temperature was kept at 70℃, and

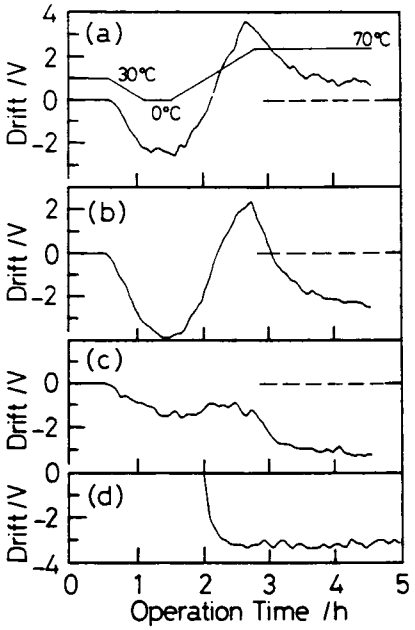

Fig. 9 Thermal drifts of the same modulator measured (a) without dc bias voltage and (b) with a 5-V dc bias. Graph (c) denotes the calculated results of (b)–(a). The dc drift of this modulator measured at 70℃ and dc = 5 V is shown in (d).

its magnitude (~ –3 V) was the same as that of the dc drift measured at 70℃ and dc = 5 V, as shown in Fig. 9(d). The relaxation times of the drift in Fig. 9(c) and 9(d) were calculated to be 18 and 16 min, respectively. These results indicated that the dc and thermal drifts were simply accumulated during operation of the modulators. Further, the relaxation time of the slow thermal drift observed during the soaking time at 70℃ [see Fig. 9(a)] was calculated to be 20 min and close to the dc drift, suggesting that both drift phenomena had similar origins.

Figures 10(a) and 10(b) show the results measured for two kinds of modulators made from different $LiNbO_3$ wafers (solid and broken lines in the figures denote the data for two different modulators from the same wafer). The measurements were carried out at 80℃ with a dc bias voltage of 5 V, which was applied in addition to the 1-kHz ac voltage of $V_{p\text{-}p}$ = 20 V. To avoid the influence of the thermal drift, the dc bias voltage was applied more than 2 hr after the sample was heated up in the oven. As can be seen, the dc drift phenomena were caused by multiple sources. The drift toward the negative direction, observed in the initial stage of the measurement, was found to have an activation energy E_a of ~0.5 eV (Ref. 18) and was considered to depend on the SiO_2 buffer layer for the following reasons. As the buffer layer thickness was increased from 500 nm [Fig. 11(a)] to 1500 nm [Fig. 11(c)], the negative drift emerged gradually. In the sample with a 500-nm-thick buffer layer [Fig. 11(a)], no negative drift was observed. Further, when the buffer layer was prepared by the rf sputtering method instead of the present vacuum evaporation method, such negative drift could not be detected between –20 and 80℃.

Figure 12 shows the other dc drift results observed at 130℃ during the follow-up bias-controlled operations, where the initial dc bias of 3.5 V (~V_π) was applied to the acdriven modulator, and the dc bias was changed to maintain the operating

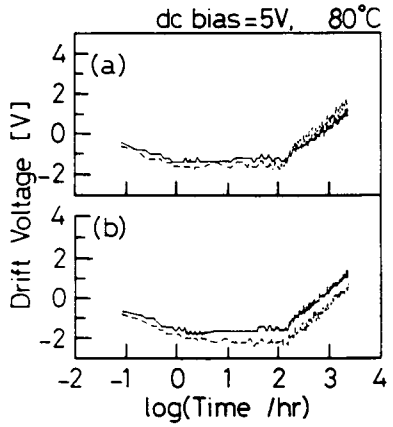

Fig. 10 (a) and (b) correspond to the dc drifts measured for each of two modulators made from two different wafers. The measurements were carried out at 80℃ and with constant dc bias voltages of 5 V.

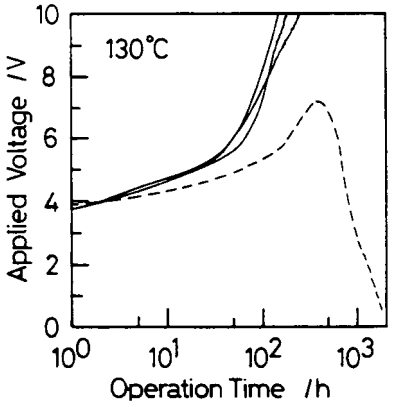

Fig. 12 The dc drift of the three different modulators (shown by solid curves) measured at 130℃ via the followup bias-controlled operations. Initially applied dc bias voltages were 3.5 V. The broken curve denotes a similar result for another modulator with a proton-reduced $LiNbO_3$ substrate.

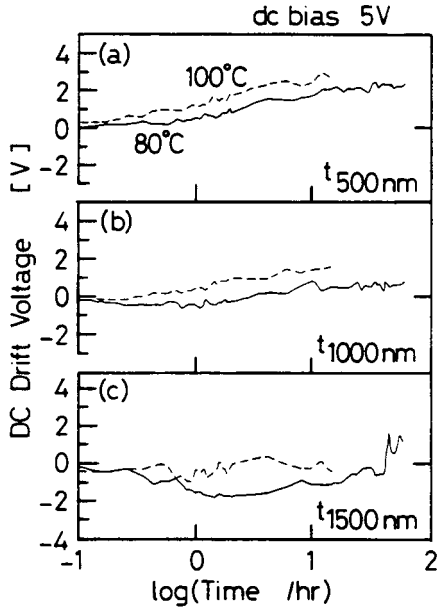

Fig. 11 The dc drift measured at dc = 5 V for three modulators with SiO_2 buffer layers 500 nm thick (a), 1000 nm thick (b), and 1500 nm thick (c).

point of the light-modulation output at the initially biased state. The control frequency was ~1 kHz. The solid curves in Fig. 12 denote the results of the present modulators made from three different wafers. The applied dc voltages increased almost proportionally to the logarithmic operation time, and their rates increased after ~40 hr of operations. The early slow drift seemed to correspond to the positive drifts of Fig. 10. The E_a of this drift was measured to be 0.8 ~ 1 eV between 60 and 130℃. The E_a of the sequential fast drift of Fig. 12 was calculated to be 0.4 eV from similar results measured at 80, 100, and 130℃.[43] These dc drift phenomena were toward a positive direction, which resulted in suppressing the applied dc bias, and were considered to be mainly due to the nature of the $LiNbO_3$ substrate, such as the proton content. The broken curves in Fig. 12 were the result measured for the modulator fabricated from the reduced proton $LiNbO_3$ wafer (mentioned in Sec. 2.1) via a dry Ti diffusion process. Such differences in the wafer led to significant reduction of the dc drift. The sources of the ultimate negative drift observed in this modulator are not known yet, because there was a possibility that the protons in the substrate (and the buffer layer) decreased further, gradually, during such a long-term storage at 130℃. Consequently, it was found for the present modulators that at least three types of dc drift appeared chronologically, which had individual E_a values. There is a possibility that the fast drift of Fig. 12 was generated by an excess dc bias application beyond 5.5 V (i.e., the existence of a threshold bias voltage for the fast dc drift mode).

4.2 *Distribution of dc Drifts in Wafers*

For routine measurements of the dc drift, the modulators were operated with the follow-up bias control circuitry (mentioned in Sec. 4.1) at 80℃ for 100 hr. As indicators of the magnitude of the drift, the absolute applied dc voltages, including an initial bias of 3.5 V at 100 hr, and the drift rates calculated from the applied voltages at 50 and 100 hr were plotted in Fig. 13(a) and 13(b), respectively. The horizontal axes of the figures denote the device chip number along the *y* direction of the wafer. The results for four different wafers were exhibited as different marks. As can be seen, the extent of the distributions both for the in-wafer and between-wafers were similar, and the extent of the dc bias distribution [see Fig. 13(a)] resulted in ~2 V for the modulators used here. The drift rates in Fig. 13(b) extended from negative to positive values, and no correlation was found between the absolute bias voltages and the drift rates as shown in Fig. 14.

These results indicated the necessity of a screening test for all modulator products. Figure 15 summarizes ~100 data points of Fig. 13(a) as frequency [f (%)] and cumulative frequency [F (%)] diagrams. In 60% of the samples, the applied dc voltages at 80℃ and 100 hr were equal, to or less than 3.5 V for the initial dc bias, suggesting these modulators exhibited the large-extent and/or long-term negative dc drift (see Fig. 10). In the screening test for the thermal drift (see Sec. 3), the test criterion could be determined as the V_π, for in-

stance, for the extent of maximum drift measured within the ordinary operating temperatures. However, the test criterion for the dc drift could not be set simply because it was related largely to the problem of device lifetime. Further, lifetime estimation was also difficult because of complex mechanisms and behaviors of the dc drift phenomenon.

If the E_a of 1 eV and a constant drift rate of 1 mV/hr [average value in Fig. 13(b)] were assumed instead of the actual operation time-dependent drift rate, applied dc biases at 40℃ and 25 years could be calculated as ~7 V, including the initial bias of 3.5 V, even for modulators which resulted in 5 V in the screening test at 80℃ for 100 hr. In this regard, all modulator products of Fig. 15 would be supplied as reduced dc drift modulators. However, as shown in Fig. 16, one could take other rather severe procedures for estimating lifetime, where the typical result measured at 130℃ (see solid curves in Fig. 12) was used to calculate the dc bias voltages in 50 and 70℃ operations. Here, the E_a value for the prior slow positive drift was set at 0.8 eV (broken curves) and 1 eV (solid curves) while that for the following fast drift was fixed at 0.4 eV, judging from the previous experimental results.[43] As can be seen, the lifetime of the present modulators in continuous 70℃ operations would be less than 2 or 3 years with ordinary driving voltages. This estimate was the worstcase one because the negative dc drift, appearing as early as the bias application, was not counted.

4.3 *Possibility of Reduced dc Drift Modulators*

As described earlier, the test procedure and criteria for choosing the reduced drift modulators remained uncertain in the applied parameters (such as E_a) and data extrapolation methods for estimating lifetime. On the other hand, concerning the reduced dc drift modulators, it was found empirically that there were desirable fabrication techniques to obtain such modulators.[44] One of them was the device consisting of a proton-reduced $LiNbO_3$ substrate thermally treated under dry atmosphere and the vacuum-evaporated SiO_2 buffer layer, whose drift behavior was shown in Fig. 12 by the broken curve. The rate of its dc drift was significantly slower than that of the present ones (solid curves) in which no attention was paid to the protons in the substrates. However, such improved drift modulators needed further investigation from the viewpoints of the drift reduction mechanism and production repeatability. Figure 17 shows the distribution of the dc drifts for the modulators fabricated from the same wafer as the one for Fig. 12. The drifts were measured at 80℃ with the constant dc bias voltages of 5 V, and the drift voltages after 15 min (open

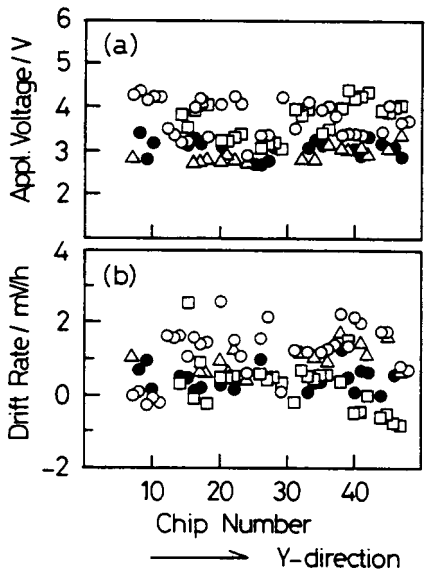

Fig. 13 Distribution of dc drift of the present modulators measured at 80℃ via the followup bias-controlled operators with initial bias voltages of 3.5 V. Horizontal axes correspond to the y direction of the wafer. (a) Distribution of the applied dc bias voltages after 100 hr of operation. (b) Distribution of the drift rates calculated from the voltages at 50 and 100 hr. The results for the modulators from the same wafer were denoted by the same marks.

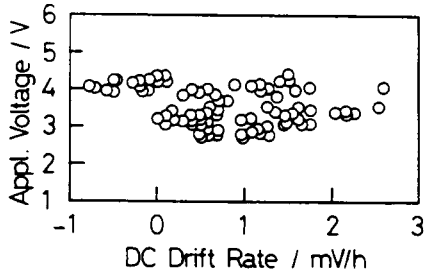

Fig. 14 Relation between the bias voltages and the drift rates of Fig. 13(a) and 13(b), respectively.

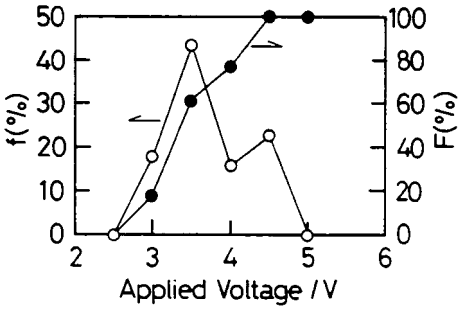

Fig. 15 Distribution of the applied voltage of Fig. 13(a) for all measured modulators. F(%) of the right vertical axis indicates a cumulative percent of the frequency f(%) for each applied voltage.

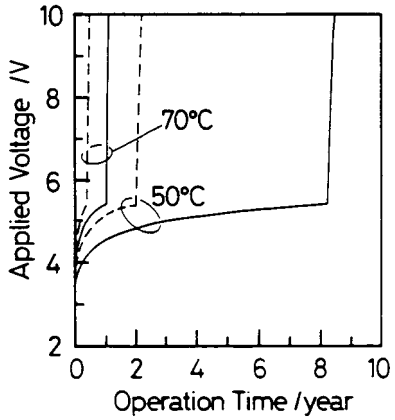

Fig. 16 The dc drift at 50 and 70℃ estimated from the measured results at 130℃ of Fig. 12 with the assumption of activation energies of 1 eV (solid curves) and 0.8 eV (broken curves). The activation energy for the latter drift of two-step dc drift in the figure was fixed to be 0.4 eV.

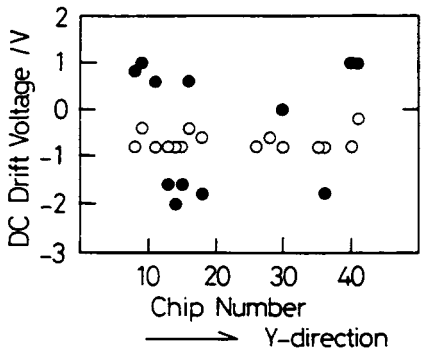

Fig. 17 Distribution of dc drift measured for modulators made from the same proton reduced wafer (the same as the sample shown in Fig. 12 by broken curve). The open and closed circles denote the drift voltages after 15 min and 90 hr of operation, respectively, at 80℃ and with dc = 5 V.

circles) and 90 hr (closed circles) operations were plotted. While the short-term drift exhibited a small range of the distribution, the longer term drift scattered greatly, depending on the device chip. In these devices, the elimination of the protons was not complete because some thermal treatments (such as the annealing of the buffer layer) and storage until their assembly processes were carried out under a conventional atmosphere (not dry), possibly leading to such a low repeatability in performance.

5 Conclusions

The reliability issues of the drift phenomena of hermetically sealed Ti:$LiNbO_3$ optical intensity modulators, which depend on the inevitable characteristics of the constituent materials rather than external problems such as device assembly techniques, have been reported. Within the present technology, the repeatable fabrication of drift-free modulators was impossible because of the uncertainty in the $LiNbO_3$ material itself. Some empirical demands in the materials and fabrication process conditions could be clarified to prepare devices with reduced thermal and dc drift. In this regard, the amounts of the proton impurities in the wafer and buffer layer had to be adjusted in addition to a fabricating suitable Mach–Zehnder waveguide design, for balancing drift-induced fluctuations of the propagating lightwave. At present, however, screening tests to choose the promising modulators with smaller drift behavior must be done since the distribution of their drift phenomena was large and could not be predicted even in the wafer unit. Concerning the dc drift, further longterm (in months) measurements at ≥ 100℃ for a few modulators cut from each wafer are desirable in order to estimate the possible dc drifts in practical operations.

Acknowledgments

The authors are thankful to Dr. J. Minowa, Mr. J. Ogiwara, M. Yamada, M. Sakuma, M. Kobayashi, H. Honda, T. Shinriki, S. Shimotsu, K. Kiuchi, T. Saito, T. Tateyama, S. Murata, S. Oikawa, T. Sugimoto, M. Shiroishi, and Dr. J. Nayyer of the Optoelectronics Division of Sumitomo Osaka Cement Co., Ltd. for helpful discussions and for device fabrication and measurements.

References

1. T. Fukuda, "Recent progress on crystals for optoelectronic applications," *Oyo Butsuri* **63**(3), 248–254 (1994).
2. N. Iyi and K. Kitamura, "Nonstoichiometry and defect structure of $LiNbO_3$." *J. Crystallographic Soc. Jpn*. **35**(6). 404–409 (1993).
3. W. A. Tiller and S. Uda, "Intrinsic $LiNbO_3$ melt species partitioning at the congruent melt composition," *J. Crys. Growth* **129**, 328–361 (1993).
4. A. Koide, H. Shimizu, and T. Saito, "Formation and chaiaclerization of Li-H out-diffused optical waveguide," *Extended Abstracts of the 54th Autumn Meeting of Jpn. Soc. Appl. Phys.* 1993, **28-p-G7**, Jpn. Soc. Appl. Phys, Tokyo (1993).
5. S. Miyazawa and J. Noda, "Problems in fabricating Ti-diffused $LiNbO_3$ optical waveguides," *Oyo Butsuri* **48**(9), 867–874 (1979).
6. M. Fontaine, A. Delage, and D. Landheer, "Modeling of titanium diffusion into $LiNbO_3$ using a depth-dependent diffusion coefficient," *J. Appl. Phys*. **60**(7), 2343–2350 (1986).
7. R. J. Holmes and D. M. Smith, "Titanium diffusion into $LiNbO_3$ as a function of stoichiometry," *J. Appl. Phys*. **55**(10), 3531–3534 (1984).
8. J. L. Jackel, V. Ramaswamy, and S. P. Lyman, "Elimination of out-diffused surface guiding in titanium-diffused $LiNbO_3$," *Appl. Phys. Lett*. **38**(7), 509–511 (1981).
9. M. De Sario, M. N. Armenise, C. Cnali. A. Camera, P. Mazzoldi, and G. Celotti, "TiO_2, $LiNb_3O_8$, and $(Ti_xNb_{1-x})\ O_2$ compound kinetics during Ti:$LiNbO_3$ waveguide fabrication in the presence of water vapors," *J. Appl. Phys*. **57**(5), 1482–1487 (1985).
10. G. E. Betts, F. J. O'Donnell, and K. G. Ray, "Effect of annealing on photorefractive damage in titanium-indiffused $LiNbO_3$ modulators," *IEEE Photonics Tech. Lett*. **61**(1), 211–213 (1994).
11. M. Seino, T. Nakazawa, Y. Kubota, M. Doi, T. Yamane, and H. Hakogi, "A low de-drift Ti:$LiNbO_3$ modulator assured over 15 years," *Proc. OFC'92*, pp.325–328, Opt. Soc. of America, Washington, DC (1992).
12. H. Kuwahara. A. Miyauchi, and A. Mitsuhashi, "Fiber optic transmission," *FUJITSU Sci. Tech. J*. **28**(2), 216–227 (1992).
13. H. Jumonji and T. Nozawa, "Instabilities and their characterization in Mach-Zehnder Ti:$LiNbO_3$ optical modulators," *IEICE Trans. Inst. Electron.* J75-C-1(1), 17–26 (1992).
14. P. Skeath, C. H. Bulmer, S. C. Hiser, and W. K. Burns, "Novel electrostatic mechanism in the thermal instability of z-cut $LiNbO_3$ interferometers," *Appl. Phys. Lett*. **49**(19), 1221–1223 (1986).
15. S. Yamada and M. Minakata, "DC drift phenomena in $LiNbO_3$ optical waveguide devices," *Jpn. J. Appl. Phys*. **20**(4), 733–737 (1981).
16. C. M. Gee, G. D. Thurmond, H. Blauvelt, and H. W. Yen, "Minimizing dc drift in $LiNbO_3$ waveguide devices," *Appl. Phys. Lett*. **47**(3), 211–213 (1985).
17. R. A. Becker, "Circuit effect in $LiNbO_3$ channel-waveguide modulators," *Opt. Lett*. **10**(8), 417–419 (1985).
18. H. Nagata and K. Kiuchi, "Temperature dependence of dc drift of Ti:$LiNbO_3$ optical modulators with sputter deposited SiO_2 buffer layer," *J. Appl. Phys*. **73**(9), 4162–4164 (1993).
19. H. Nagata, J. Ichikawa, M. Kobayashi, J. Hidaka, H. Honda, K. Kiuchi, and T. Sugamata, "Possibility of dc drift reductin of Ti:$LiNbO_3$ modulators via dry O_2 annealing process," *Appl. Phys. Lett*. **64**(10), 1180–1182 (1994).
20. H. Nagata. K. Kiuchi, S. Shimotsu, J. Ogiwara, and J. Minowa, "Estimation of direct current bias and drift of Ti:$LiNbO_3$ optical modulators," *J. Appl. Phys*. **76**(3), 1405–1408 (1994).
21. Y. Urino, N. Kitamura, T. Kanbe, and H. Nishimoto, "DC drift phenomenon caused by hydrogen in $LiNbO_3$ substrate," *Extended Abstracts of the 54th Autumn Meeting of Jpn. Soc. Appl. Phys. 1993* **28p-G-3**, Jpn. Soc. Appl. Phys., Tokyo (1993).
22. N. Mekada, M. Seino, Y. Kubota, and H. Nakajima, "Practical method of waveguide-to-fiber connection: direct preparation of waveguide endface by cutting machine and reinforcement using ruby beads," *Appl. Opt*. **29**(34), 5096–5102 (1990).
23. M. Minakata, T. Yonai, and K. Yamada, "DC drift free Ti diffused $LiNbO_3$ optical modulators," *Technical Digest of OEC'94* pp. 19–21, **PDII-3**, IEICE, Tokyo (1994).
24. R. G. Smith, D. B. Fraser, R. T. Denton, and T. C. Hich, "Correlation of reduction in optically induced refractive-index inhomogeneity with OH content in $LiTaO_3$ and $LiNbO_3$," *J. Appl. Phys*. **39**(10), 4600–4602 (1968).
25. W. Bollmann and H.-J. Stohr, "Incorporation and mobility of OH^- ions in $LiNbO_3$ crystals," *Phys. Stat. Sol. (a)* **39**, 477–484 (1977).
26. D. P. Birnie III, "Hydrogen defects and optical damage in $LiNbO_3$," in *Ceramics and Inorganic Crystals for Optics, Electro-Optics, and Nonlinear Conversion. Proc. SPIE* **68**, 81–87 (1988).
27. A. Forster, S. Kapphan, and M. Wohlecke, "Overtone spectroscopy of OH and OD stretch modes in $LiNbO_3$," *Phys. Stat. Sol. (b)* **143**, 755–764 (1987).
28. J. R. Herrington, B. Dischler, A. Rauber, and J. Schneider, "An optical study of the stretching absorption band near 3 microns from OH^- defects in $LiNbO_2$," *Solid State Commun.* **12**, 351–354 (1973).
29. L. Kovacs, V. Szalay, and R. Capelletti, "Stoichiometry dependence of

the OH^- absorption band in $LiNbO_3$ crystals," *Solid State Commun.* **12**, 1029–1031 (1984).
30. L. Kovacs, M. Wohlecke, A. Javnovic, K. Polgar, and S. Kapphan, "Infrared absorption study of the OH vibrational band in $LiNbO_3$ crystals," *J. Phys. Chem. Solids* **52**(6), 797–803 (1991).
31. A. Koide, H. Shimizu, and T. Saito, "Study of mode formation in Ti:$LiNbO_3$ optical waveguide: proton in crystal and water vapor atmosphere," *Extended Abstracts of the 55th Autumn Meeting of Jpn. Soc. Appl. Phys*., pp. 964, **22a-R-1** Jpn. Soc. Appl. Phys, Tokyo (1994).
32. C. E. Rice and R. J. Holmes, "A new rutile structure solid-solution phase in the $LiNb_3O_8$-TiO_2 system, and its role in Ti diffusion into $LiNbO_3$," *J. Appl. Phys*. **60**(11), 3836–3839 (1986).
33. M. N. Armenise, C. Canali, M. De Sario, A. Carnera, P. Mazzoldi, and G. Celotti, "Characterization of TiO_2, $LiNb_3O_8$, and ($Ti_{0.65}Nb_{0.35}O_2$) compound growth observed during Ti:$LiNbO_3$ optical waveguide fabrication," *J. Appl. Phys*. **54**(11), 6223–6231 (1983).
34. M. A. McCoy, S. A. Dregia, and W. E. Lee, "Crystallography of surface nucleation and epitaxial growth of lithium triniobate on congruent lithium niobate," *J. Mater. Res*. **9**(8), 2029–2039 (1994).
35. M. A. McCoy, S. A. Dregia, and W. E. Lee, "Evolution of phases and microstructure in optical waveguides of lithium niobate," *J. Mater. Res*. **9**(8), 2040–2050 (1994).
36. H. Nagata, K. Kiuchi, and T. Saito, "Refractive index fluctuations in deformed Ti:$LiNbO_3$ waveguides due to overlayer deposition," *Appl. Phys. Lett*. **63**(9), 1176–1178 (1993).
37. J. Ogiwara and E. Suzuki, "Cutting and polishing procedures of $LiNbO_3$ substrates for optical devices," *Extended Abstracts of the Autumn Meeting of Jpn. Soc. Precision Engineering 1990*, pp. 625–626, JSPE, Tokyo (1990).
38. H. Nagata, K. Kiuchi, and T. Saito, "Studies of thermal drift as a source of output instabilities in Ti:$LiNbO_3$ optical modulators," *J. Appl. Phys*. **75**(9), 4762–4764 (1994).
39. H. Nagata, M. Shiroishi, Y. Miyama. N. Mitsugi, and N. Miyamoto, "Evaluation of new UV-curable adhesive material for stable bonding between optical fibers and waveguide devices: problems in device packaging," *Optical Fiber Technology* **1**, 283–288 (1995).
40. J. Nayyer and H. Nagata, "Suppression of thermal drifts of high speed Ti:$LiNbO_3$ optical modulators," *IEEE Photonics Tech. Lett*. **6**(8), 952–955 (1994).
41. S. K. Korotky, J. J. Veselka, C. T. Kemmerer, W. J. Minford, D. T. Moser, J. E. Watson, C. A. Mattoe, and P. L. Stoddard, "High-speed, low power optical modulator with adjustable chirp parameter," *Technical Digest of IPR'91*, pp. 53–54 TuG2, Opt. Soc. of America, Washington, DC (1991).
42. J. Nayyer, H. Nagata, S. Shimotsu, S. Oikawa, and J. Minowa, "Modulation characteristics of high speed optical modulators with properly split asymmetry into their Mach-Zehnder arms," *Electron. Lett*. **31**(5), 387–388 (1995).
43. H. Nagata and J. Nayyer, "Stability and reliability of lithium niobate optical modulators," *Technical Digesi of IPR'95*, pp. 290–292, Opt. Soc. of America, Washington, DC (1995).
44. H. Nagata, H. Takahashi, H. Takai, and T. Kougo, "Impurity evaluation of SiO_2 films formed on $LiNbO_3$ substrates," *Jpn. J. Appl. Phys*. **34**(2), 606–609 (1995).

Hirotoshi Nagata received his BS in inorganic materials engineering from the Nagoya Institute of Technology in 1984 and DEng in materials science from Tokyo Institute of Technology in 1992. He joined Central Research Laboratories of Sumitomo Osaka Cement Co., Ltd. in 1984. He is engaged in research and development of ceramics materials and films. Since 1992 he has been investigating reliability and quality issues of lithium niobate-based optical modulator devices at the Optoelectronics Division of SUmitomo.

Junichiro Ichikawa received his BS and MS degrees in mineralogy from the University of Tokyo in 1987 and 1989, respectively. He joined the Optoelectronics Division of Sumitomo Osaka Cement Co., Ltd. in 1989 and is engaged in research and development of lithium niobate-based devices. His recent interest is epitaxial film growth of lithium niobate and its application to optical devices.